Video Article

Whole-brain Segmentation and Change-point Analysis of Anatomical Brain MRI—Application in Premanifest Huntington's Disease

Dan Wu[1], Andreia V. Faria[1], Laurent Younes[2,3,4], Christopher A. Ross[5], Susumu Mori[1,6], Michael I. Miller[2,3,7]

[1]The Russell H. Morgan Department of Radiology and Radiological Science, Johns Hopkins University School of Medicine

[2]Center for Imaging Science, Johns Hopkins University

[3]Institute for Computational Medicine, Johns Hopkins University

[4]Department of Applied Mathematics and Statistics, Johns Hopkins University

[5]Division of Neurobiology, Departments of Psychiatry, Neurology, Neuroscience and Pharmacology, and Program in Cellular and Molecular Medicine, Johns Hopkins University School of Medicine

[6]F.M. Kirby Research Center for Functional Brain Imaging, Kennedy Krieger Institute

[7]Department of Biomedical Engineering, Johns Hopkins University

Correspondence to: Dan Wu at dwu18@jhu.edu

URL: https://www.jove.com/video/57256
DOI: doi:10.3791/57256

Keywords: Medicine, Issue 136, Change-point, MRI atlas, segmentation, granularity, MRICloud, premanifest HD

Date Published: 6/9/2018

Citation: Wu, D., Faria, A.V., Younes, L., Ross, C.A., Mori, S., Miller, M.I. Whole-brain Segmentation and Change-point Analysis of Anatomical Brain MRI—Application in Premanifest Huntington's Disease. *J. Vis. Exp.* (136), e57256, doi:10.3791/57256 (2018).

Abstract

Recent advances in MRI offer a variety of useful markers to identify neurodegenerative diseases. In Huntington's disease (HD), regional brain atrophy begins many years prior to the motor onset (during the "premanifest" period), but the spatiotemporal pattern of regional atrophy across the brain has not been fully characterized. Here we demonstrate an online cloud-computing platform, "MRICloud", which provides atlas-based whole-brain segmentation of T1-weighted images at multiple granularity levels, and thereby, enables us to access the regional features of brain anatomy. We then describe a regression model that detects statistically significant inflection points, at which regional brain atrophy starts to be noticeable, *i.e.* the "change-point", with respect to a disease progression index. We used the CAG-age product (CAP) score to index the disease progression in HD patients. Change-point analysis of the volumetric measurements from the segmentation pipeline, therefore, provides important information of the order and pattern of structural atrophy across the brain. The paper illustrates the use of these techniques on T1-weighted MRI data of premanifest HD subjects from a large multicenter PREDICT-HD study. This design potentially has wide applications in a range of neurodegenerative diseases to investigate the dynamic changes of brain anatomy.

Video Link

The video component of this article can be found at https://www.jove.com/video/57256/

Introduction

Magnetic resonance imaging (MRI) has substantially enhanced our ability to examine the brain anatomy and functions in neurodegenerative diseases[1,2,3]. T1-weighted structural MRI is one of most widely adopted imaging tools in routine clinical practice to assess the brain anatomy and related pathology. Quantitative analysis of the high-resolution T1-weighted images provides useful markers to measure anatomical changes during brain degeneration. In particular, segmentation based quantification approaches effectively reduces the image dimensionality from voxel level (on the order of (10^6)) to anatomical structural level ((10^2)) for high-throughput neuroinformatics[4,5]. Automated brain segmentation can be achieved using atlas-based methods[6,7,8,9] that map the pre-defined anatomical labels from an atlas onto the patient images. Among the atlas-based methods, multi-atlas algorithms[10,11,12,13,14] have yielded superior segmentation accuracy and robustness. Our group has developed a fully automated T1 multi-atlas segmentation pipeline, with advanced diffeomorphic image registration algorithms[15], multi-atlas fusion methods[16,17], and rich multi-atlas libraries[18]. The pipeline has been distributed on a cloud-computing platform, MRICloud[19], since 2015, and it has been used to study neurodegenerative diseases, such as Alzheimer's disease (AD)[20,21], Primary Progressive Aphasia[22], and Huntington's Disease[23].

Once the high-resolution images are segmented into brain structures, regional features, such as volumes, can be used to establish mathematical models to characterize the neuroanatomical changes. A change-point analysis method was recently established by our group to analyze the temporal order, in which statistically significant brain morphometric changes occur, based on longitudinal and/or cross-sectional MRI data. This statistical model was first developed to quantify shape-based diffeomorphometry over age in AD patients[21,24]; and it was later adapted to investigate brain structural changes in Huntington's disease (HD), as well as to describe brain developmental changes in neonatal brains[25]. In HD patients, the change-point was defined in with respect to the CAG-age product (CAP) score, as an indicator of the extent of exposure to the CAG expansion in *HTT*[26]. It is well-known that striatal atrophy is one of the earliest markers in HD, followed by the globus pallidus[27]. Yet, the changes in striatum in relation to other gray and white matter structures across the brain remains unclear. Such relation is crucial for us to

understand the disease progression. Change-point analysis of volumetric changes in all brain structures will likely provide systematic information of brain atrophy in premanifest phase of HD.

Here we demonstrate the procedures to perform whole-brain segmentation using MRICloud (www.mricloud.org), and steps to perform change-point analysis of volumetric data in premanifest HD subjects. The MRI data were collected from a large population multicenter PREDICT-HD study[28,29] with approximately 400 controls and premanifest HD subjects. The combination of atlas-based segmentation and change-point analysis brings unique information about the spatiotemporal order of the brain structural changes and the disease progression pattern across the brain. The techniques are potentially applicable to a range of neurodegenerative diseases with various biomarkers to map the brain degeneration.

Protocol

1. Atlas-based Whole Brain Segmentation

1. **Data preparation**
    1. Convert three-dimensional (3D) T1-weighted images, typically acquired with MPRAGE (magnetization-prepared rapid gradient-echo) sequence, from vendor-specific DICOM (Digital Imaging and Communication) format to Analyzed format. Note that the cloud computation requires users' data to be transferred to remote clusters. According to the Health Insurance Portability and Accountability Act (HIPPA), remove the patients' personal identification information from the image files.
    NOTE: MRICloud offers a DICOM-to-Analyze converter (https://braingps.mricloud.org/t1prep) for the file format conversion as well as the de-identification of personal health information.
        1. Double-click to open Dcm2Analyze.exe. A popup window will open (**Figure 1A**).
        2. Specify the input DICOM data directory path as input and Analyzed image path and file name as output.
        3. Click "Go" to complete the conversion.
        NOTE: The conversion needs to be performed for each individual patient, and it would be beneficial to output all converted images in one study folder for batch processing (1.2.2.1).

2. **Multi-atlas based T1 image segmentation using MRICloud[19].**
    1. Log-in "Brain GPS" (register for first-time users) from https://mricloud.org. Select "Segmentation" tool from the main menu (**Figure 1B**). There are two application programming interface (API) options under "Segmentation": "T1-MultiAtlas" for single T1 image segmentation, and "T1-MultiAtlas Batch" for batch processing. The change-point analysis requires large population data, and thereby, batch processing is often the choice.
    2. Submit jobs on "T1-MultiAtlas Batch" API.
        1. Compress multiple Analyzed image files into a zip file. Click "+.zip" in **Figure 1B** to upload the zip file.
        NOTE: The current cloud portal limits the number of images to 30 in each zip folder. Large datasets can be separated into multiple zip folders to be processed. Special request can be made to accommodate more images per zip file. In the future, we may potentially increase the limited number or even remove the limit when more remote computational resources become available.
        2. Fill in the required fields in **Figure 1B**.
            1. Processing server: Choose "Computational Anatomy Science Gateway".
            2. Slice Type: Choose from "Sagittal", "Axial", or "Sagittal converted to Axial".
            NOTE: "Sagittal" refers to images acquired with sagittal orientation with in-plane view in Anterior-Posterior and Head-Foot directions. "Axial" refers to images acquired axial orientation with in-plane view in Left-Right and Anterior-Posterior directions. "Sagittal converted to Axial" refers to images that were originally acquired in axial orientation but later converted to sagittal images (those are typically "Axial" images with long neck area).
            3. Multi-atlas library: Choose the atlas library with closest age range to the user data to optimize the segmentation accuracy. We provide prebuilt multi-atlas datasets[18] with different age ranges, e.g., "Pediatric 4-8yr", "Pediatric 8-12yr", "Adult 22-50", and "Adult 50-90", as well as different atlas versions. Information about atlas versions can be found in https://braingps.mricloud.org/atlasrepo.

    3. Check the job status through "My job status" (**Figure 1C**). Once the jobs are finished, a "Download Results" button will appear that allows users to download the segmentation results as a .zip file.
    4. Visualize the results. For single subject, the volumes obtained from the segmentation result can be visualized online (not feasible for batch processing results).
        1. Click "View result" button in **Figure 1C**. The webpage will turn to the visualization interface (**Figure 1D**). The axial, sagittal, and coronal views of the segmentation map are overlapped on the T1-weighted anatomical image. 3D rendering of the segmented brain structures are shown in the upper left window. Color of the overlaying segmentation map indicates the z-score of the structural volumes.
        2. Adjust the visualization options, including overlay ON/OFF, opacity of the overlay, zoom in and out, and slice positions from the upper right panel in **Figure 1D**.
        3. Group finest segmentation parcels into different granularity. In our atlases, we defined five levels of granularity with two types ontology relations[18,30]. A tree-view of the hierarchical multi-level anatomical definitions is shown in the lower left panel (**Figure 1D**). Click the level numbers to expand the structures at the corresponding ontology level. The segmentation maps will simultaneously switch to the corresponding ontology level.
        NOTE: Bi-monthly MRICloud workshops are help at Johns Hopkins University School of Medicine to offer hands-on tutorials of the online operations described above. Workshop Information can be found from https://braingps.mricloud.org/workshops.

5. Download the segmentation results for subsequent analysis. Unzip the results to a user study directory, e.g., put together the segmentation results from all the subjects in one study directory, each in their individual subject folders.
NOTE: The results include

- example.img: original T1 image in axial orientation.
- example_MNI.img: T1 image in MNI space following the Talairach coordinates.
- example_7Labels.img and example_7Labels_MNI.img: Coarse segmentation with 7 parcels (gray matter, white matter, cerebrospinal fluid, lateral ventricle, skull, and background) in native and MNI space, respectively.
- example_283Labels_M2.img and example_283Labels_M2_MNI.img: fine segmentation with 283 parcels (atlas version V9B) in native and MNI space, respectively. The exact number of labels depends on the atlas version.
- example_corrected_MNI_stats.txt and example_MNI_stats.txt: statistics of volumes of each brain parcels in native and MNI space.
- multilevel_lookup_table.txt: Multilevel ontology definition of the brain parcels.

3. **Perform batch processing to obtain brain volumes in a population. Use an in-house Matlab (www.mathworks.com) batch processing script to extract brain volumes from individual result folders and combine the volumetric data of all subjects at all granularity levels to a spreadsheet. A graphic user interface (GUI) is used to specify the input and output.**
    1. Open Matlab.exe, run Main.fig, and a GUI will pop out (**Figure 2A**).
    2. In the "T1 Volume extraction from MRICloud" panel (upper panel in **Figure 2A**), specify the inputs, including the study directory where the downloaded the segmentation results are saved (see 1.2.5); and the multi-level lookup table file path and file name.
    3. Specify the output spreadsheet file path and file name where the volume data will be write to.
    4. Click "Extract volume" button to run the analysis. Results can be checked in the user-defined spreadsheet.
    NOTE: In addition, an R package is developed to process the MRICloud outputs and perform further statistical analysis, provided by Dr. Brian Caffo[31]. The package can be downloaded from https://github.com/bcaffo/MRIcloudT1volumetrics.

2. Change-point Analysis of Volumetric Data

NOTE: Please refer the theory and mathematical details of the change-point model to our previous publications[21,24,23]. Briefly, for HD data, a regression model is established to define a critical change-point (in terms of CAP score), starting from which, the linear regression between CAP and volume becomes statistical significant, while correcting for the effects of patient's age, gender, and intracranial volume. In-house Matlab scripts, along with a GUI (**Figure 2A**, lower panel), was developed to compute the change-points for individual structures and perform statistical analysis. The scripts are available to users upon request.

1. **Calculate change-points for individual brain structures.**
    1. In the "Change-point analysis" panel in **Figure 2A**, specify the file path and name of the multilevel volume spreadsheet, which is generated according to 1.3.
    2. Specify the file path and name of the output text file, which the change-point results will be written to.
    3. Choose the level of granularity and type of ontology definition in the drop-down box (Level 1 - 5), at which the change-point analysis will be performed.
    4. Click "Calculate change-point" button to perform the change-point analysis, as described in reference[23], and the resultant change-points will be saved in the output text file.

2. **Statistical evaluations of the change-points.**
    1. In the Matlab GUI (**Figure 2A**, lower panel), specify parameters for statistical tests, including the number of permutation (default 10,000), number of bootstrap (default 10,000), and p-value threshold (after the FDR correction, default 0.05).
    2. Click "Statistical test" button to run the tests. After this step, the p-value (by permutation test), before and after false-discovery rate (FDR) correction, as well as the standard deviation and the 95% confidence interval (by bootstrap) of the change-points will be written to the output text file as extra columns. See details of statistical test procedures in[23,24].

3. Generate change-point maps (optional). In the Matlab GUI (**Figure 2A**, lower panel), click "Map change-point" button to generate change-point maps. Statistically significant change-point values will be mapped onto the MNI-space anatomical image to visualize the spatial pattern. This mapping can be done at different granularity levels, depending on the anatomical level specified in 2.1. The change-point maps can be overlaid on T1-weighted images using MRIcro (**Figure 2B**) (http://www.cabi.gatech.edu/mricro/mricro/).

Representative Results

Using the procedures described in 1.1-1.3, whole brain segmentation maps can be obtained from MRICloud. In the current version of atlas (V9B), 283 parcels are segmented at the finest granularity (level 5), which can be grouped to different levels of granularity, *e.g.*, from hemisphere to lobules and parcels, according to specific ontology definitions. **Figure 3** shows two types of multi-level segmentations at five levels, in axial and coronal views. For example, at the coarsest level, Type-I segmentation defines classical brain regions of the telencephalon, diencephalon, mesencephalon, metencephalon, and myelencephalon (**Figure 3A**), while Type-II defines clinically and radiologically used conventions of hemispheres, cerebellum, and brainstem (**Figure 3B**). Here, we use Type-II definitions for the following analysis, and we average the volumes from the left and right hemispheres, as there is no known laterality in HD pathology.

Change-point analysis of the brain volumes is performed based on the segmentation results, according to section 2.1-2.2. In **Figure 4**, we take the basal ganglia as an example to examine the related change-points at different granularity levels. The 3D hierarchical structural definitions of basal ganglia are illustrated in the top row. Scatter plots of change-point analysis in individual structures are shown in the bottom row, where the blue dots denote the z-scores of the structural volumes from the premanifest HD patients (normalized to controls), after correcting for age, sex, and intracranial volumes; the black curves are the fitted volume z-scores, regressed to the change-point component in the model[23]; and the red lines indicates the positions of the detected change-points. At level 1, only hemispherical separation is available, and the corresponding scatter plot shows the whole hemisphere has a gradual atrophy as CAP score increases, with a change-point at CAP of 360 and 95% confidence interval of [352.8, 367.2] ($p = 0.011$ after FDR correction). At level 2, the basal ganglia is a part of the cerebral nuclei, and the cerebral nuclei shows a change-point at CAP of 232 [227.7, 236.3] ($p < 0.01$ after FDR). At level 3, basal ganglia is an independent structure and it shows a change-point at CAP of 233 [228.6, 237.4] ($p < 0.01$ after FDR). At level 4, basal ganglia is divided into the striatum and the globus pallidus, which have change-points at CAP of 230 [225.6, 234.4] and 243 [238.6, 247.4], respectively (both $p < 0.01$ after FDR). At level 5, the striatum is further divided into caudate and putamen, which show change-points at CAP of 240 [234.9, 245.1] and 211 [206.8, 215.2], respectively (both $p < 0.01$ after FDR).

Once the individual change-points are calculated for all brain structures, whole-brain spatial maps of the change-points can be obtained according to 2.3. **Figure 5** shows the change-point maps at different granularity levels with Type-II ontological definitions. Note that only the structures with significant change-points ($p < 0.05$ after FDR correction) are mapped. At level 1, the entire brain parenchyma (except cerebellum) shows a significant but relatively late change-point at CAP of 360 [352.8, 367.2] ($p = 0.011$ after FDR); whereas the cerebrospinal fluid (CSF, including lateral ventricle, III and IV ventricle, and sulci space) shows a slightly earlier change point at CAP of 319 [313.0, 325.0] ($p=0.022$ after FDR). The regions with significant change-points become more localized as the granularity level goes higher, and the spatial variance begins to unveil. For example, at level 3, the inferior white matter exhibits an earlier change-point (CAP = 305 [298.8, 311.2], $p = 0.038$ after FDR), compared to the anterior white matter (CAP = 371 [363.9, 378.1], $p = 0.042$ after FDR). At level 5, the differences among putamen, caudate, and globus pallidus become noticeable, with the putamen showing the earliest change-point, followed by the caudate and globus pallidus.

The change-rates are calculated as the percentage of volumetric changes (normalized to healthy controls) per CAP score, after the change-point. The change-rates of the corresponding structures are mapped in **Figure 6**, where the warm colors indicate volume increases in ventricles and sulci CSF and the cold colors indicate volume decreases in the brain parenchyma. At level 3, the deep gray matter structures show highest change rate, followed by the anterior white matter, and then inferior white matter. At level 5, the putamen and globus pallidus exhibit the fastest atrophy (0.1% volumetric loss per CAP), followed by the caudate (0.07% per CAP). As the granularity goes higher, the change-rates become higher in more localized regions.

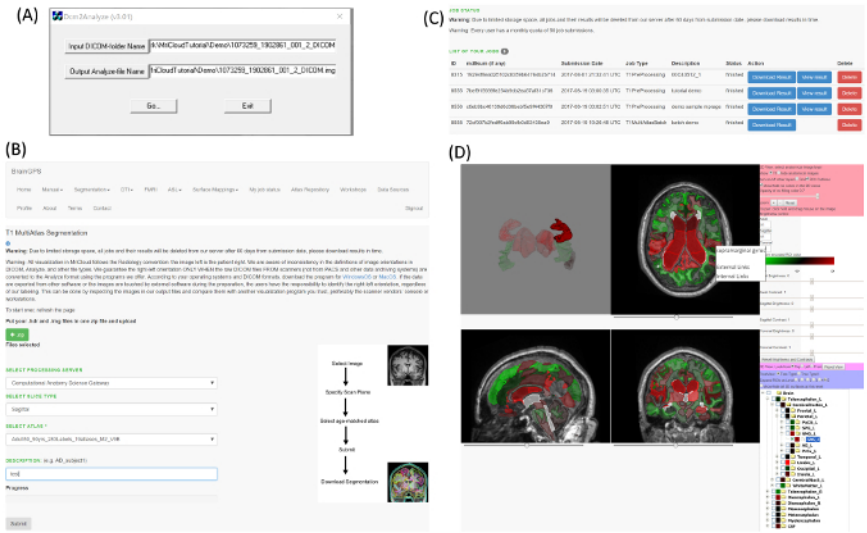

Figure 1: Illustration of T1-weighted image segmentation on MRICloud. (**A**) Use of Dcm2Analyzed.exe to convert DICOM files to Analyzed format and perform de-identification. (**B**) Webpage for "T1-MultiAtlas Batch" processing. (**C**) Webpage for "My job status". (**D**) Webpage for visualization of segmentation results. Please click here to view a larger version of this figure.

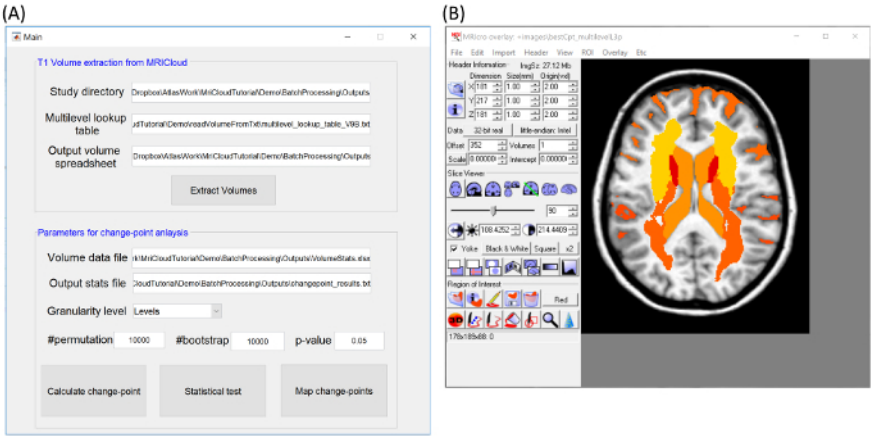

Figure 2: Graphic User Interface (GUI) to perform volume analysis and change-point analysis. (**A**) Matlab GUI for batch extraction of volumetric data from MRICloud segmentation outputs (upper panel) and change-point analysis (lower panel). (**B**) MRICro interface to visualize the change-point maps. Please click here to view a larger version of this figure.

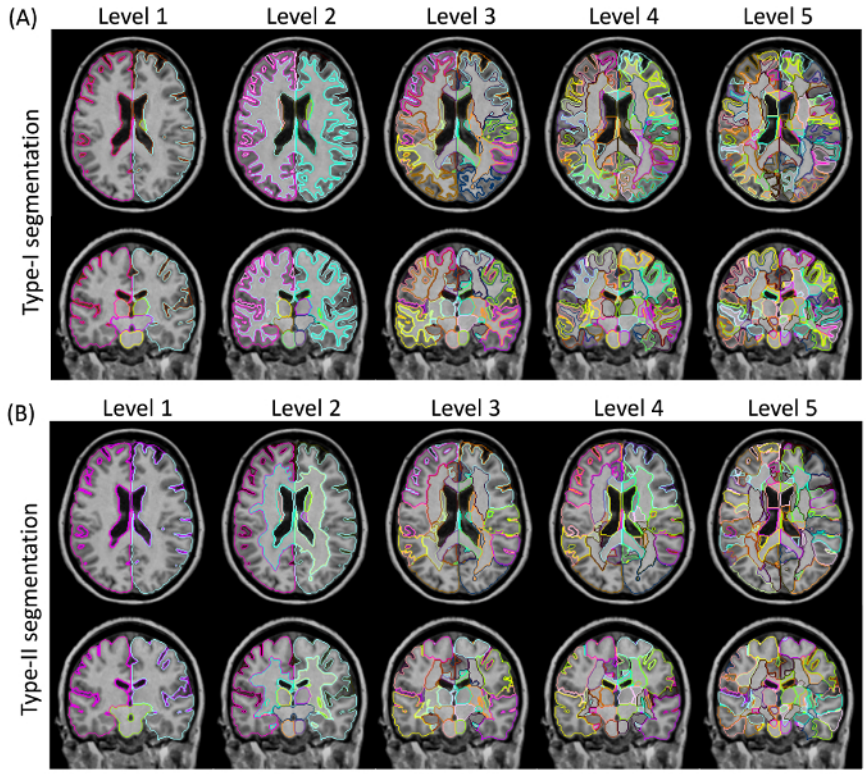

Figure 3: Atlas-based whole brain segmentation at multiple granularity levels with two types of ontological relationships. Axial and coronal views of multi-level segmentation maps are overlaid on T1-weighted anatomical images, according to Type-I (**A**) and Type-II (**B**) ontological definitions. Please click here to view a larger version of this figure.

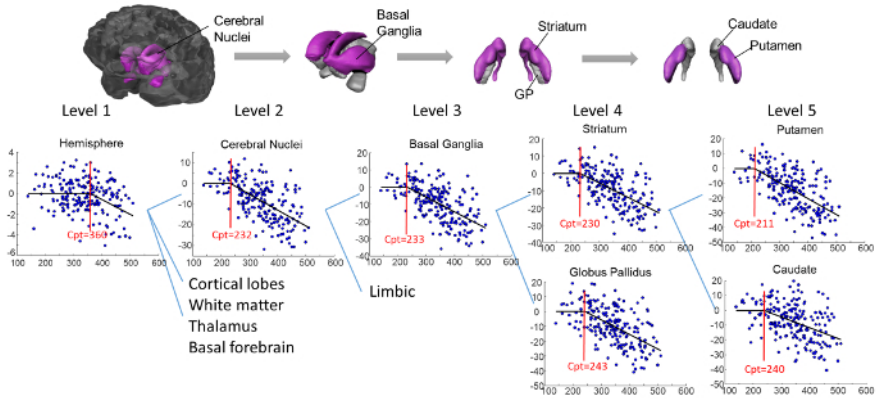

Figure 4: Change-point analysis of the basal ganglia at multiple granularity levels. The hierarchical anatomical relations between hemisphere (level 1), cerebral nuclei (level 2), basal ganglia (level 3), striatum and globus pallidus (level 4), and putamen and caudate (level 5) are illustrated in the top row with 3D rendering. The scatter plots demonstrate change-point analysis of these structures, where the blue dots denote the z-scores of volumetric data (normalized to healthy controls) after correcting for age, sex, and intracranial volumes; the black curves are the fitted z-scores, regressed to the change-point dependent CAP component; and the red lines indicate the positions of the change-points. Please click here to view a larger version of this figure.

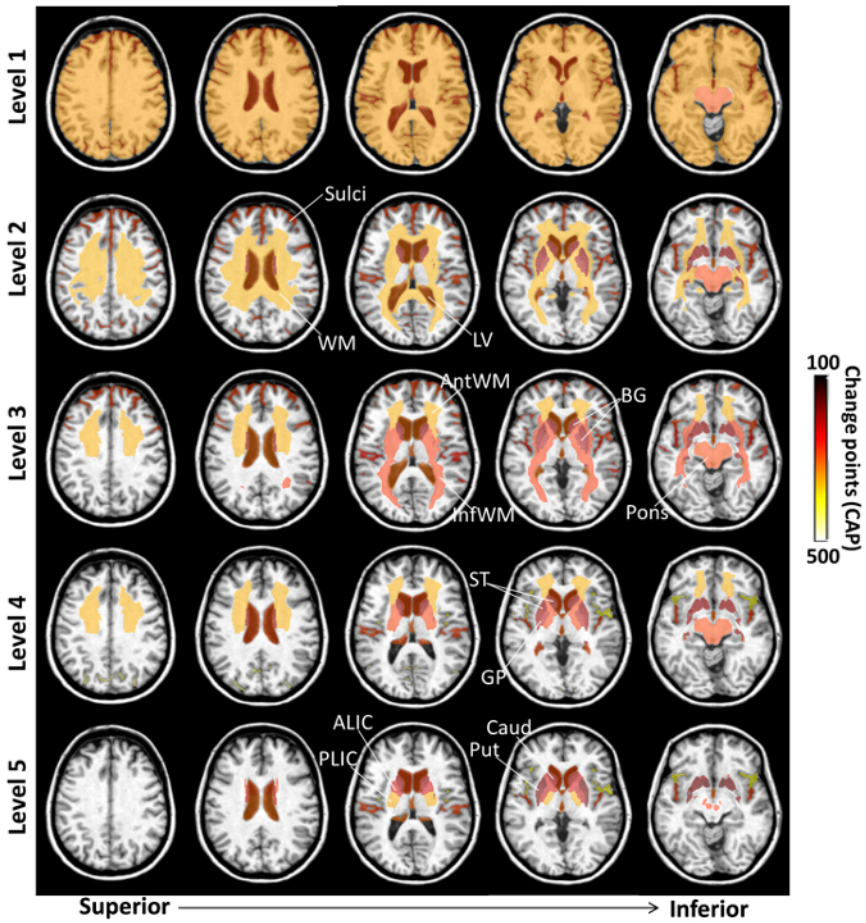

Figure 5: Whole brain change-point maps at multiple granularity levels. The regions that show significant change points (at 5% FDR) are mapped onto a T1-weighted image, and the colors indicate the change-point values in unit of CAP score. Abbreviations: WM:white matter; LV: lateral ventricle; AntWM: anterior white matter; InfWM: inferior white matter; BG: basal ganglia; ST: striatum; GP: globus pallidus; ALIC: anterior limb of the internal capsule; PLIC: posterior limb of the internal capsule; Caud: caudate; Put: putamen. Please click here to view a larger version of this figure.

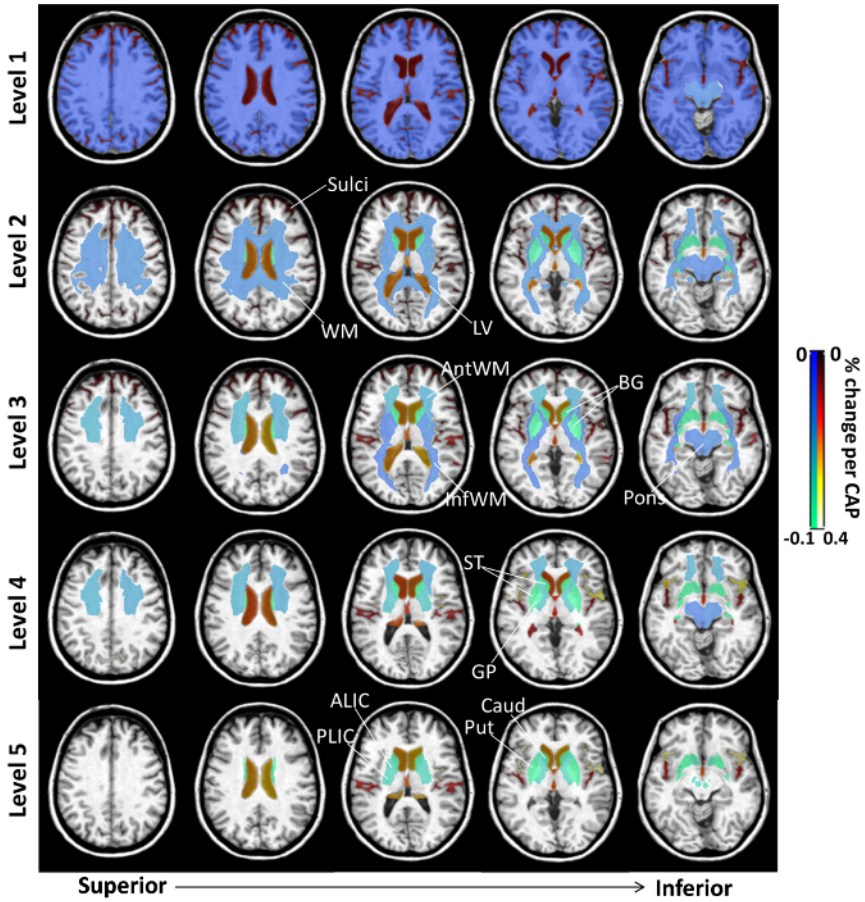

Figure 6: Whole brain change-rate maps at multiple granularity levels. Change-rates are calculated as the percentage of volume changes per CAP, after the change-point (normalized to healthy controls), in the regions that show significant change-points (at 5% FDR), mapped onto a T1-weighted image. Abbreviations: WM: white matter; LV: lateral ventricle; AntWM: anterior white matter; InfWM: inferior white matter; BG: basal ganglia; ST: striatum; GP: globus pallidus; ALIC: anterior limb of the internal capsule; PLIC: posterior limb of the internal capsule; Caud: caudate; Put: putamen. Please click here to view a larger version of this figure.

Discussion

As demonstrated in this paper, whole-brain segmentation of brain MRI can be conveniently achieved using our online platform MRICloud. T1-weighted MRI based volumetric marker has shown to be robust and sensitive to a range of neurodegenerative diseases[1,2,3]. The volumetric measures are used for various downstream analysis, such as mathematical modeling, and feature-selection and classification analysis to assist clinical diagnosis and prognosis. Change-point analysis of brain volumes allows quantitative characterization of brain atrophy during disease progression. This statistical analysis employs a regression model with a nonlinear component to define a change-point in the course of brain atrophy over a disease index, *e.g.*, CAP score in HD. Compared to conventional group analysis that is widely adopted in most existing studies, the change-point model seeks for the exact onset points of brain atrophy, and therefore, offers more specific information of brain degeneration. Combining with an automated whole-brain segmentation pipeline, spatial maps of the change-points can be obtained, which reveal the spatiotemporal pattern of disease progression in HD. This is especially important in the premanifest phase of HD when therapeutic interventions can be most effective.

In the multi-atlas based image segmentation, brain segmentations at multiple granularities are provided to make the volumetric analysis flexible and scalable to various studies. For example, for Alzheimer's disease, several small brain structures are of particular interest, such as Hippocampus, Amygdala, or subdivisions of the temporal cortex; whereas for frontotemporal dementia, brains are examined at relatively coarse scales, such as the entire frontal and temporal lobes. According to our previous study[33], the segmentation precision and reproducibility may be compromised at high granularity. In addition, the statistical challenge for multiple comparison would increase at higher granularity, as shown in **Figure 5**. In addition, an appropriate choice of atlas libraries, depending on age range and disease types of the study, is important for the segmentation accuracy[18,32]. The change-point analysis requires a relatively large number of data to perform the regression analysis, *e.g.*, n >50 is usually needed based on empirical experience. Interpretation of change-point results heavily relies on the statistical test, because the model will produce a change-point for any dynamic data series, which sometimes is insignificant. We used a permutation test to evaluate whether the addition of change-point significantly reduces the model's residual error, and we used the bootstrap operation to mitigate the influence of outliers.

There can be variations to the change-point model depending on specific applications. For example, the disease index, which is CAP score for HD patients, can be replaced with other clinical variables, or simply age. Other covariates can also be included in the model, such as imaging protocols[23] and other factors to be accounted for. Furthermore, the model is applicable to various types of biomarkers beyond volumetric marker, including other imaging markers (from different contrast mechanisms such as diffusion, perfusion, or functional MRI) and non-imaging markers.

In addition, the mathematical formulation of the model can be adapted according to different assumptions and hypotheses. For examples, the model can involve a baseline linear regression before the change-point and an additional linear regression that occurs after the change-point, such as proposed in reference[24].

The proposed change-point analysis in combination atlas-based whole-brain segmentation can have wide applications in both clinical and basic science studies of neurodegenerative diseases. Yet, there are limitations with the proposed techniques. The dynamic changes of biomarkers may not be linear, and thereby, linear component used in the current change-point model may not be optimal. Generalized linear model can potentially be integrated to handle nonlinear situations. Secondly, the change-point analysis requires large population longitudinal and/or cross-sectional data, such as the multi-center PREDICT-HD data used in this study. Different image acquisition protocols, from multi-center studies or longitudinal studies, may impose a bias in the volume measurements. Our multi-atlas image segmentation pipeline has shown to be relatively robust to protocol differences, compared to biological effects, such as age and pathology[34]. Still, it may be necessary to remove the protocol difference beforehand, or to include the protocol effect as one of the covariates in the change-point model as described in[23]. Currently, downstream volumetric analysis is not included in MRICloud, and users will need to extract volumes from the segmentation maps or use our Matlab toolbox to perform the multi-granularity volume analysis. We can potentially integrate this offline processing step into the cloud pipeline in the future, if this is identified as a common request by users.

The proposed change-point analysis in combination atlas-based whole-brain segmentation can have wide applications in both clinical and basic science studies of neurodegenerative diseases.

Disclosures

The authors have nothing to disclose.

Acknowledgements

We thank the PREDICT-HD investigators, particularly, Dr. Hans Johnson and Dr. Jane S. Pauslen from University of Iowa, for their generosity in sharing the MRI data and constructive discussion on the data analysis and results.

This work is supported by NIH grants R21 NS098018, P50 NS16375, NS40068, R01 NS086888, R01 NS084957, P41 EB015909, P41 EB015909, R01 EB000975, R01 EB008171, and U01 NS082085.

References

1. Paulsen, J. S. *et al.* Clinical and Biomarker Changes in Premanifest Huntington Disease Show Trial Feasibility: A Decade of the PREDICT-HD Study. *Front Aging Neurosci.* **6** 78 (2014).
2. Jack, C. R., Jr. *et al.* Hypothetical model of dynamic biomarkers of the Alzheimer's pathological cascade. *Lancet Neurol.* **9** (1), 119-128 (2010).
3. Laakso, M. P. *et al.* Hippocampal volumes in Alzheimer's disease, Parkinson's disease with and without dementia, and in vascular dementia: An MRI study. *Neurology.* **46** (3), 678-681 (1996).
4. Miller, M. I., Faria, A. V., Oishi, K., & Mori, S. High-throughput neuro-imaging informatics. *Front Neuroinform.* **7** 31 (2013).
5. Mori, S., Oishi, K., Faria, A. V., & Miller, M. I. Atlas-based neuroinformatics via MRI: harnessing information from past clinical cases and quantitative image analysis for patient care. *Annu Rev Biomed Eng.* **15** 71-92 (2013).
6. Klein, A., Mensh, B., Ghosh, S., Tourville, J., & Hirsch, J. Mindboggle: automated brain labeling with multiple atlases. *BMC Med Imaging.* **5** 7 (2005).
7. Heckemann, R. A., Hajnal, J. V., Aljabar, P., Rueckert, D., & Hammers, A. Automatic anatomical brain MRI segmentation combining label propagation and decision fusion. *Neuroimage.* **33** (1), 115-126 (2006).
8. Artaechevarria, X., Munoz-Barrutia, A., & Ortiz-de-Solorzano, C. Combination strategies in multi-atlas image segmentation: application to brain MR data. *IEEE Trans Med Imaging.* **28** (8), 1266-1277 (2009).
9. Lotjonen, J. M. P. *et al.* Fast and robust multi-atlas segmentation of brain magnetic resonance images. *Neuroimage.* **49** (3), 2352-2365 (2010).
10. Rohlfing, T., Brandt, R., Menzel, R., & Maurer, C. R. Evaluation of atlas selection strategies for atlas-based image segmentation with application to confocol microscopy images of bee brains. *Neuroimage.* **21** (4), 1428-1442 (2004).
11. Fischl, B. *et al.* Whole brain segmentation: Automated labeling of neuroanatomical structures in the human brain. *Neuron.* **33** (3), 341-355 (2002).
12. Collins, D. L., Holmes, C. J., Peters, T. M., & Evans, A. C. Automatic 3-D model-based neuroanatomical segmentation. *Human Brain Mapping.* **3** (3), 190-208 (1995).
13. Dawant, B. M. *et al.* Automatic 3-D segmentation of internal structures of the head in MR images using a combination of similarity and free-form transformations: Part I, methodology and validation on normal subjects. *Ieee Transactions on Medical Imaging.* **18** (10), 909-916 (1999).
14. Wu, G. *et al.* A generative probability model of joint label fusion for multi-atlas based brain segmentation. *Med Image Anal.* **18** (6), 881-890 (2014).
15. Miller, M. I., Trouve, A., & Younes, Y. Diffeomorphometry and geodesic positioning systems for human anatomy. *Technology.* **2** (2013).
16. Tang, X. *et al.* Bayesian Parameter Estimation and Segmentation in the Multi-Atlas Random Orbit Model. *PLoS One.* **8** (6), e65591 (2013).
17. Wang, H. *et al.* Multi-Atlas Segmentation with Joint Label Fusion. *IEEE Trans Pattern Anal Mach Intell.* **35** (3), 611-623 (2013).
18. Wu, D. *et al.* Resource atlases for multi-atlas brain segmentations with multiple ontology levels based on T1-weighted MRI. *Neuroimage.* **125** 120-130 (2015).
19. Mori, S. *et al.* MRICloud: Delivering High-Throughput MRI Neuroinformatics as Cloud-Based Software as a Service. *Computing in Science & Engineering.* **18** (5), 21-35 (2016).

20. Wu, D., Ceritoglu, C., Miller, M. I., & Mori, S. Direct estimation of patient attributes from anatomical MRI based on multi-atlas voting. *Neuroimage-Clinical.* **12** 570-581 (2016).
21. Miller, M. I. *et al.* Network Neurodegeneration in Alzheimer's Disease via MRI Based Shape Diffeomorphometry and High-Field Atlasing. *Front Bioeng Biotechnol.* **3** 54 (2015).
22. Faria, A. V. *et al.* Content-based image retrieval for brain MRI: an image-searching engine and population-based analysis to utilize past clinical data for future diagnosis. *Neuroimage Clin.* **7** 367-376 (2015).
23. Wu, D. *et al.* Mapping the order and pattern of brain structural MRI changes using change-point analysis in premanifest Huntington's disease. *Hum Brain Mapp.* (2017).
24. Younes, L., Albert, M., Miller, M. I., & Team, B. R. Inferring changepoint times of medial temporal lobe morphometric change in preclinical Alzheimer's disease. *Neuroimage Clin.* **5** 178-187 (2014).
25. Wu, D. *et al.* Mapping the critical gestational age at birth that alters brain development in preterm-born infants using multi-modal MRI. *NeuroImage.* **149** 33-43 (2017).
26. Zhang, Y. *et al.* Indexing disease progression at study entry with individuals at-risk for Huntington disease. *Am J Med Genet B Neuropsychiatr Genet.* **156b** (7), 751-763 (2011).
27. Vonsattel, J. P. *et al.* Neuropathological classification of Huntington's disease. *J Neuropathol Exp Neurol.* **44** (6), 559-577 (1985).
28. Paulsen, J. S. *et al.* Detection of Huntington's disease decades before diagnosis: the Predict-HD study. *J Neurol Neurosurg Psychiatry.* **79** (8), 874-880 (2008).
29. Paulsen, J. S. *et al.* Prediction of manifest Huntington's disease with clinical and imaging measures: a prospective observational study. *Lancet Neurol.* **13** (12), 1193-1201 (2014).
30. Djamanakova, A. *et al.* Tools for multiple granularity analysis of brain MRI data for individualized image analysis. *Neuroimage.* **101** 168-176 (2014).
31. Caffo, B. *A package for T1 volumetric analysis of MRIcloud output. R package version 0.0.1.*, <https://github.com/bcaffo/MRIcloudT1volumetrics> (2017).
32. Aljabar, P., Heckemann, R. A., Hammers, A., Hajnal, J. V., & Rueckert, D. Multi-atlas based segmentation of brain images: atlas selection and its effect on accuracy. *Neuroimage.* **46** (3), 726-738 (2009).
33. Unified Huntington's Disease Rating Scale: reliability and consistency. Huntington Study Group. *Mov Disord.* **11** (2), 136-142 (1996).
34. Liang, Z. *et al.* Evaluation of Cross-Protocol Stability of a Fully Automated Brain Multi-Atlas Parcellation Tool. *PLoS One.* **10** (7), e0133533 (2015).

